

Effect on microstructure of TiO₂ rate in Al₂O₃-TiO₂ composite coating produced using plasma spray method

S. ISLAK*, S. BUYTOZ^a, E. ERSOZ^a, N. ORHAN^a, J. STOKES^b, M. SALEEM HASHMI^b,
I. SOMUNKIRAN^a, N. TOSUN^a

Cide Rifat Ilgaz Vocational High School, Kastamonu University, 37600 Kastamonu, Turkey

^a*Metallurgy and Materials Engineering, Technology Faculty, Firat University, 23119 Elazig, Turkey*

^b*School of Mechanical and Manufacturing Engineering, DCU, Dublin, Ireland*

In this study, Al₂O₃-TiO₂ composite coatings were thermally sprayed on the SAE 1040 steel using atmospheric plasma spray (APS) process of mixed different rates micron-sized TiO₂ and micron-sized Al₂O₃ powders. The effects of TiO₂ addition on the microstructure, phase compositions and microhardness of the coatings were investigated by using scanning electron microscopy (SEM), energy dispersive spectroscopy (EDS), X-ray diffractometry (XRD) and microhardness tester. The results show that the Al₂O₃-TiO₂ composite coatings consists of both fully melted regions and partially melted regions, and the fully melted region has a lamellar-like structure. Phase transformations from mainly stable α -Al₂O₃ and anatase-TiO₂ in the powders to predominant metastable γ -Al₂O₃, rutile-TiO₂ and Al₂TiO₅ phase in the Al₂O₃-TiO₂ composite coatings were observed. It was determined that the pore content decreased with the increased in the TiO₂ powder rate. The microhardness of the coating layers was 3-4.5 times higher than substrate material. The average microhardness values of the coatings were found to reach 650-860 HV.

(Received May 15, 2012; accepted September 20, 2012)

Keywords: Plasma spray, Ceramic coating, γ -Al₂O₃, Rutile-TiO₂

1. Introduction

Plasma-sprayed ceramic coatings are widely used for structural applications in order to improve resistances to wear, friction, corrosion and oxidization [1]. In atmospheric plasma spraying (APS) one of many plasma spray methods, a coated layer is formed on a substrate surface by spraying melted powders onto a substrate at a high speed using a high-temperature plasma jet [2,3]. Powder grains are transported within a carrier gas at high-temperature and high speed, injected into plasma jet. The melting powder is transferred to the substrate surface being coated and after impact, lamellar layer formation occurs [4]. Optimization of spray parameters is important for obtaining high-quality coating. In conventional plasma spray coatings, Argon (Ar) is used as the carrying gas. However, oxygen is also used as carrier gas in high-temperature plasma jet for the metal oxide powders to minimize decomposition of the metal oxide powder and the plasma coated material, as it improves the heat transfer characteristics of plasma during the spraying process [5]. Insufficient melting can occur if powder particles are too large. Optimum grain size and distribution affect the melting point of the material, the spray system used and application method of the coating [6]. In previous studies, it was determined that the microstructure of the coating material depending not only on the characteristics of the thermal spray powder but also on the hot spraying conditions [7-9].

Al₂O₃, Al₂O₃ + TiO₂, NiAl, NiCrAl and ZrO₂ ceramic coatings produced by plasma spraying are well known against wear and maintain resistance to corrosion under certain conditions [10-13]. Alumina coatings are an abrasion resistance coating example widely used in the cutting tool industry. Al₂O₃-coated tool steel was found to be 2.5 times more resistant than uncoated tool steels [12]. When TiO₂ is added to Al₂O₃, the toughness of the coating improves without changing the hardness. As the melting temperature of TiO₂ is lower, the melting point of Al₂O₃ lowers because TiO₂ can easily be connected to Al₂O₃ grains [3]. This improves coating performance.

Most researchers focus on the microstructural characteristics, and mechanical properties such as wear behavior, corrosion and oxidization behaviors of Al₂O₃-TiO₂ composite coatings. However, sufficient attention wasn't paid for the microstructural formation mechanism. Thus, the present study discusses the effects of TiO₂ addition on the microstructure, porosity of the coating layers and microhardness of Al₂O₃-TiO₂ composite coatings. In the present research, microstructure developments and chemical composition of the coating layers were examined by scanning electron microscopy (SEM), X-ray diffraction (XRD), and X-ray energy dispersive spectroscopy (EDS).

2. Experimental procedure

In this study, the substrate used for coatings was SAE

1040 steel with dimensions of 20 mm in diameter and 100 mm in height. The chemical composition (wt.%) of substrate was: C: 0.039, Si: 0.25, Mn: 0.72, P: 0.04, S: 0.05 and Fe as the balance. Commercially available, blended feedstock powder was used Al₂O₃ (melting point: 2070 °C) powder and TiO₂ (melting point: 1830 °C) powder. The mixed rates of powders used in the coatings are given in Table 1. Prior to deposition, samples were sand blasted to provide surface roughness for better adherence between the ceramic coating and metallic substrate. An average 50 µm thick bond layer of NiCr 80/20 was applied on the surface of the steel substrate to obtain better performance of the plasma sprayed Al₂O₃-TiO₂ coating.

Table 1. Characteristics and coat thicknesses of the samples.

Sample	Mix rate of powders (wt.%)		Top coat thickness (µm)	Bond coat thickness (µm)
	Al ₂ O ₃	TiO ₂		
S ₁	100	-	250	50
S ₂	97	3		
S ₃	87	13		
S ₄	60	40		

Plasma spraying was conducted on the substrate by a Sulzer Metco 9MB spray system, and argon combined with hydrogen was used as fuel gas. The schematic diagram of the plasma spray process is shown in Fig. 1. Detailed plasma spraying conditions are listed in Table 2. Ar was used as the plasma working (primary) gas. Ar gas was also used as carrier gas for the feedstock during plasma spraying with the Sulzer Metco 9MB. The substrate was fixed in front of the plasma gun at a distance 75 mm. The plasma spraying process was achieved in ambient air. The arc current was fixed at 500 A and the arc voltage was 60-80 V. The macrophotograph of the coatings produced by plasma spray process which shows the remarkable color change of the surfaces of coatings as a result of TiO₂ addition as given in Fig. 2.

Table 2. Atmospheric plasma spraying parameters.

Spraying parameters	
Plasma spray gun type	Sulzer-Metco 9MB
Arc current (A)	500
Arc voltage (V)	60-80
Working gas flow rate (l/min)	35-73
H ₂ gas flow rate (l/min)	6.6
Spray distance (mm)	75
Carrier gas flow rate (Ar) (%)	9-11.4

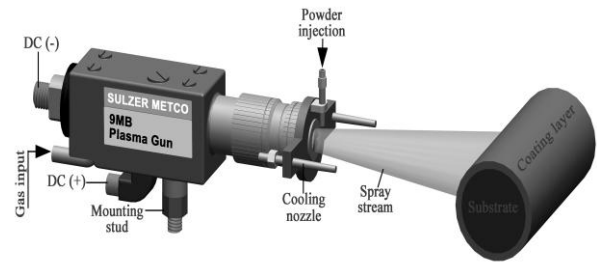


Fig. 1. Schematic picture of plasma spray coating.

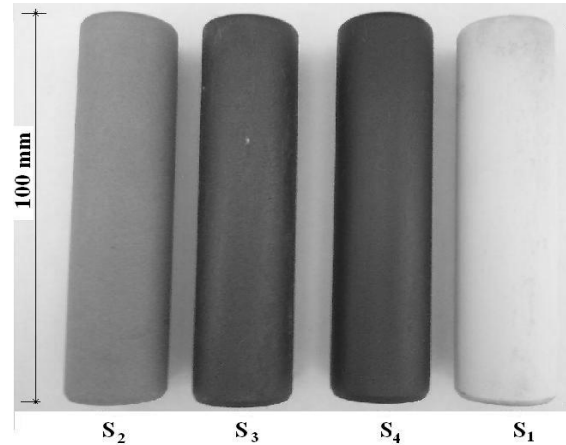


Fig. 2. Macrophotographs of coating specimens.

The specimens were polished metallographically and etched with 98 ml HNO₃ + 2 ml ethanol solution for metallographic examinations. The microstructural features of the specimens were examined with the help of scanning electron microscope (SEM) (JEM-2100F, JEOL, Japan) fitted with an energy dispersion X-ray spectroscopy (EDS) and the phases were found by X-ray diffraction (Bruker AXS D8 Advanced System, Germany). Microhardness was measured using a Future-Tech FM 700 tester with a load of 100 g and a loading time of 10 s, and porosity was determined by analyzing images photographed by optical microscope.

3. Results and discussion

3.1. Feedstock powder/coating characterization

SEM micrographs and X-ray diffraction patterns of: Al₂O₃, Al₂O₃/3wt.% TiO₂, Al₂O₃/13wt.% TiO₂, and Al₂O₃/40wt.% TiO₂ powders are shown in Fig. 3. Al₂O₃ and TiO₂ powders are different grain sizes, irregular and sharp-edged (Fig. 3). NiCr powder used as bonding layer had a partly spherical appearance (Fig. 4). As was evident from the XRD data in Fig. 3, while the pure Al₂O₃ powder consisted of α-Al₂O₃, the 3%TiO₂, 13%TiO₂ and 40% TiO₂ + Al₂O₃ alloyed powders consist of a dense α-Al₂O₃ and rutile-(TiO₂) phases.

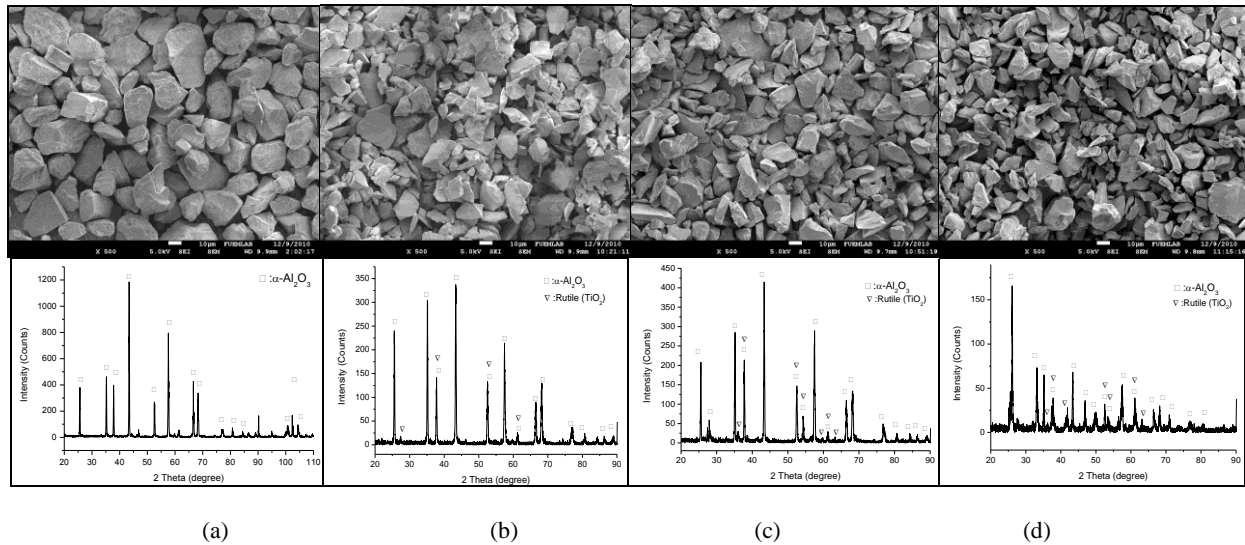


Fig. 3. SEM micrographs and XRD diffraction patterns of powders (a) 100% Al_2O_3 , (b) Al_2O_3 –3% TiO_2 , (c) Al_2O_3 –13% TiO_2 (d) Al_2O_3 –40% TiO_2 powders.

3.2. Microstructure of the coatings

The coating powder incurred three stages in plasma spraying systems. In the first stage, powder was injected into the plasma jet. In the second stage, powder was melted by plasma flame and in the third and final stage; molten powder was directed onto the surface where it rapidly solidified following the impact to the surface. Powder on the substrate can exist in three different states: unmelted, semi melted and melted. Normally, the amount of non melted powder is negligible due to the high temperature produced by plasma flame. Therefore, the microstructural occurrences after plasma spraying are discussed considering semi melted and melted particles.

The SEM micrographs of the coatings produced by plasma spray method, Al_2O_3 (100) % and Al_2O_3 - TiO_2 (97-3 %, 87 -13 % and 60-40%), are given in Figs 5 and 6. There were 3 different layers seen in Fig. 5, namely ceramic layer, intermediate layer and substrate. All coating layers were on average 300 μm and bond layers (80/20 NiCr) were approximately 50 μm thick. Pores were observed in all coating layers, (Fig. 5). Porosity in all oxide layers were determined by image analyses as approximately 6 %, which is consistent with the previous studies [13-15].

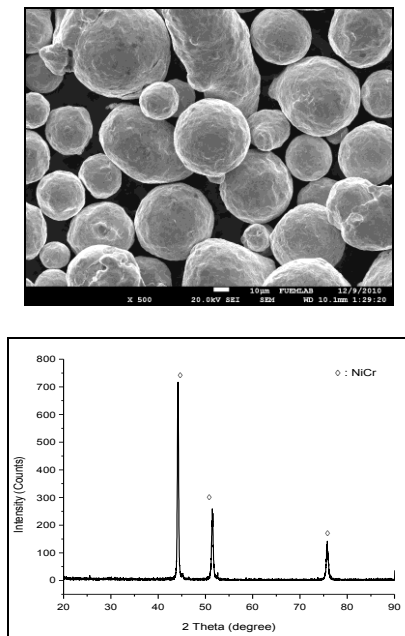


Fig. 4. SEM micrograph and EDX analyses of NiCr powder.

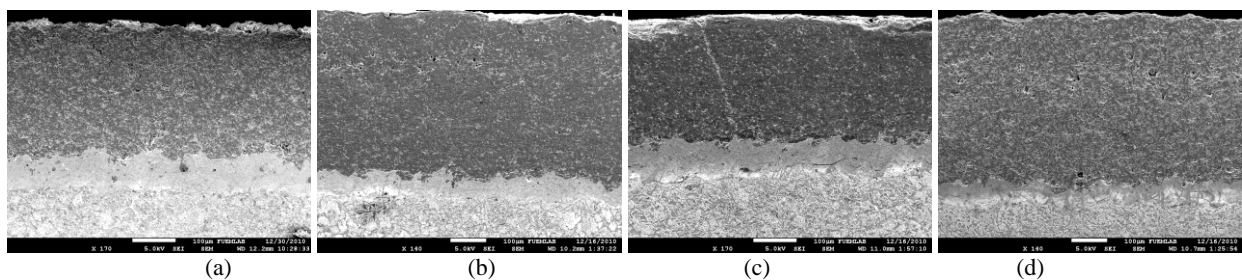


Fig. 5. Cross-sectional SEM morphologies of (a) 100% Al_2O_3 coating, (b) Al_2O_3 - 3% TiO_2 coating, (c) Al_2O_3 - 13% TiO_2 coating and (d) Al_2O_3 - 40% TiO_2 coating.

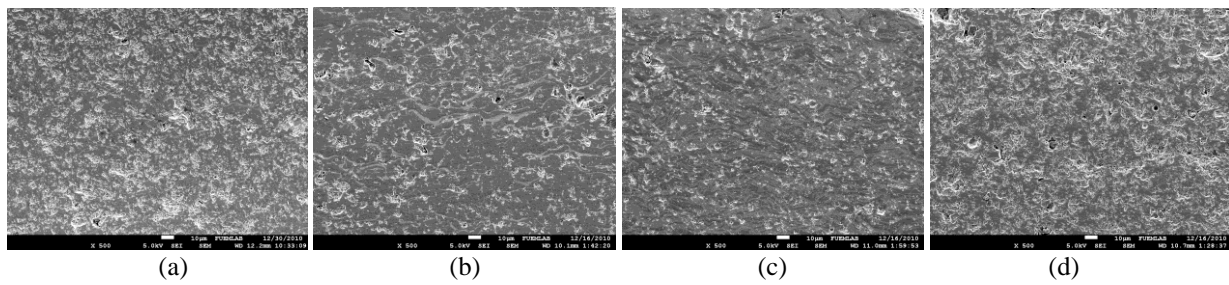


Fig. 6. SEM morphologies of Al₂O₃-TiO₂ coatings of (a) 100% Al₂O₃ coating, (b) Al₂O₃- 3% TiO₂ coating, (c) Al₂O₃- 13% TiO₂ coating and (d) Al₂O₃ - 40% TiO₂ coating.

All hot spray coatings have generally porous structures. Porosity is caused by the lack of insufficient surface wetting of the melted particles striking rough substrate surface [16]. In addition, porosity changes depending on the surface roughness of the substrate, spraying distance, initial temperature of the substrate and coating thickness [17]. Any inconsistency or difference in the thermal and mechanical properties between coating layer and substrate are reported to have caused cracking [18]. Since there were neither macro nor micro cracks observed within the coating layer in the study (Figs. 2 and 5), it was concluded that the parameters and matching materials chosen were quite proper for this coating process.

In this study, the porosity changed only with the amount of TiO₂ since the operation parameters were kept constant. From the SEM micrographs in Fig. 6, it can be seen that the porosity increased with TiO₂ content, as reported in some of the previous studies [19, 20]. But in a study by Vargas et al. [21] porosity was reported to decrease with the increase in TiO₂ content in Al₂O₃-TiO₂ based coatings on AISI 304 stainless steel substrates performed by plasma spraying and this was related to the composition of the mixture becoming closer to the eutectic composition in Al₂O₃-TiO₂ binary phase diagram (Fig. 7) as a result of the increase in TiO₂ content [22]. The particles within the powder fully melted when the flame temperature of jet was above 2040 °C and consequently formed fully melted regions forms as can be seen in Fig. 6. If the temperature is between 1854 °C and 2040 °C, TiO₂ will melt but not Al₂O₃. Since the melting temperatures of Ti and Al 1854 and 2040 °C respectively, a liquid phase sintering by melted TiO₂ will form. This will cause porosity and a weak connection between the particles due to the aggregation of Al₂O₃ particles in the liquid phase [23].

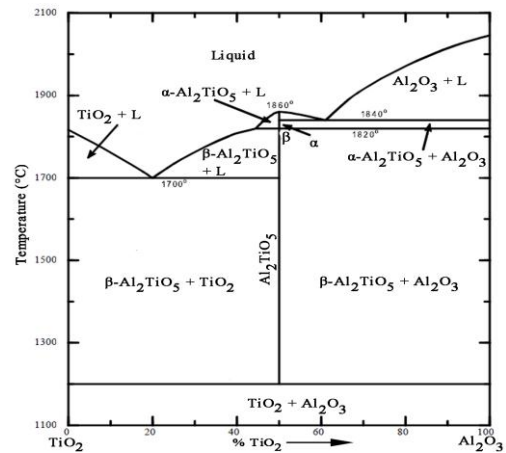


Fig. 7. Al₂O₃-TiO₂ binary phase diagram [25].

Fig. 6 shows SEM micrographs of the coated regions of Al₂O₃-TiO₂. Plasma spray coatings generally contain pores, oxides, unmelted or semi melted particles and some inclusions [24]. In this study, from Figs. 6 (b) and 6 (c), it can be seen that coating layer had a lamellar solidified structure parallel to the interface. This structure was formed as a result of the impact, deformation and solidification of the melted particles on the surface [25, 26]. Ceramic particles melt instantly without aggregation due to a very short time, less than 1/1000 second, within the plasma jet. Perpendicular spread of the particles to splat borders inferred a very good melting and spreading during the spraying [27]. Bolelli et al. [28] reported that TiO₂ partly melted and helped Al₂O₃ particles adhere better to the surface, thus resulting in a lamellar solidified structure with locally different TiO₂ composition in an Al₂O₃-13%TiO₂ coating by plasma spraying. SEM micrograph of Al₂O₃ - %40 TiO₂ coating as shown in Fig. 8 where lamellar structure, pores, partly and fully melted regions can be observed clearly.

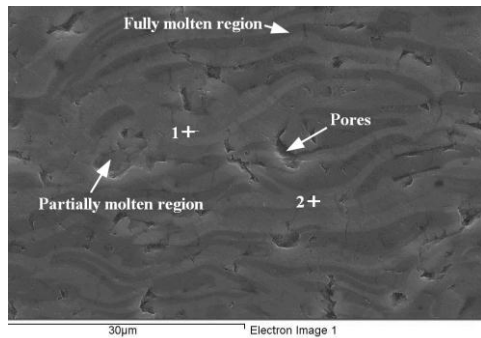


Fig. 8. SEM micrograph of Al_2O_3 - 40% TiO_2 ceramic coating layer.

Table 3. EDS analyses of Al_2O_3 and Al_2O_3 - TiO_2 coating layers.

No	EDX region	Elements (wt.%)				
		C	O	Al	Ti	Au
S ₁	1	5.75	48.38	43.48	-	2.39
	2	-	-	-	-	-
S ₂	1	2.01	46.36	41.70	7.94	1.98
	2	2.27	47.04	47.27	1.08	2.34
S ₃	1	3.98	47.77	10.96	35.07	2.21
	2	3.22	45.15	47.18	1.97	2.23
S ₄	1	1.40	46.72	10.05	39.56	2.27
	2	2.65	46.37	14.86	33.64	2.49

All coating layers were examined by EDS to determine the compositions of different phases and these phases, which are pointed 1 and 2 in Fig. 8, were shown only in one specimen since they were all present in all coated specimens. The results are given in Table 3. From Table 3, it can be seen that Al_2O_3 coating layer contained: 43.48 % Al, 48.38 % O, 2.39 % Au and 5.75 % C. The dominant phase is Al_2O_3 in the specimen S₁. Since a lamellar structure with different colour contrast occurred in the specimens coated by 3, 13 and 40 % TiO_2 , namely the specimens S₂, S₃ and S₄ as can be seen in Fig. 8, of the different colored regions, EDS data were collected. Light grey lamellar areas were rich in Al, and darker areas rich both in Al and Ti (Table 3). The more TiO_2 , the more Ti that was observed.

XRD pattern of the ceramic oxide layer produced by plasma spraying method are given in Fig. 9. From the XRD graph of the specimen coated by α - Al_2O_3 powder, the main phase was γ - Al_2O_3 and there were some α - Al_2O_3 phase. Rico et al. stated that α - Al_2O_3 phase transforms into γ - Al_2O_3 due to the low nucleation energy after spraying [29]. In the specimens coated by Al_2O_3 with different TiO_2 contents, XRD data give Al_2TiO_5 , and TiO_2 (rutile) phases beside γ - Al_2O_3 and α - Al_2O_3 phases depending on the amount of TiO_2 , (Fig. 9). With the increase in TiO_2 content, Al_2TiO_5 peaks became clearer, which was expected considering it contained the Al_2O_3 - TiO_2 binary phase diagram (Fig. 7). Before spraying, Al_2O_3 and TiO_2 powders were blended and homogenized to prevent agglomeration. Due to very small size of the particles, the

contact area among them were very large and during plasma spraying this large area caused the formation of Al_2TiO_5 reaction phase whose thermal expansion coefficient was too small and therefore it was desired for the applications where thermal resistance was needed [30-32].

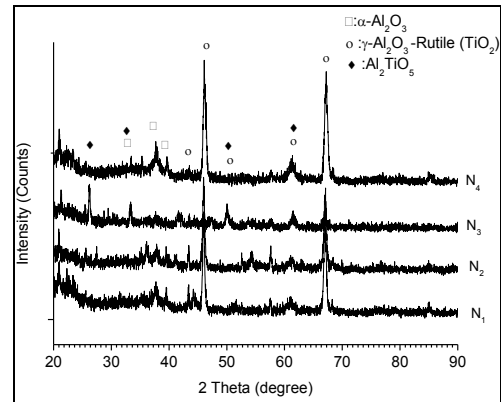


Fig. 9. XRD pattern of the coating layers.

3.3. Microhardness of the coatings

Microhardness distributions measured through three different coating layers of Al_2O_3 - TiO_2 (97-3 %, 87-13 % and 60-40 %) and Al_2O_3 (100 %) coated specimens are given in Fig. 10. The measurements were performed at least 7 points in the coating layer and their average was recorded. The hardness of the layer consisted of 100% Al_2O_3 as 877 $\text{Hv}_{0.1}$. Hardness of the coating layer decreased with increasing TiO_2 content because Al_2O_3 was harder than TiO_2 [33]. In comparison to the substrate, the microhardness of the coatings produced using plasma spray process were 3-4.5 times harder. In the fully melted regions, less porosity and higher Al_2O_3 content cause a higher hardness profile [34]. However, the coatings containing unmelted particles exhibited higher hardness due to the more α - Al_2O_3 phase rather than γ - Al_2O_3 or poor cohesion forces [35]. XRD results given in Fig. 9 prove this. Hardness varied due to variation of microstructural differences, porosity and phase distribution [20].

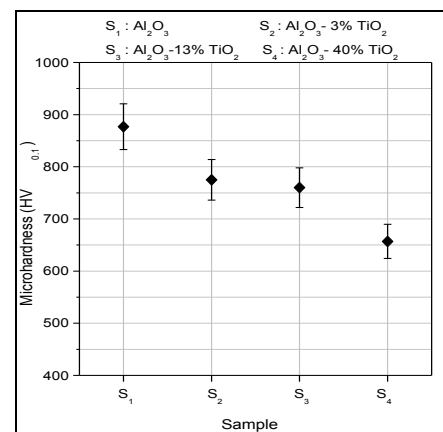


Fig. 10. Microhardness values of the coating layers.

4. Conclusions

AISI 1040 steel substrate was coated with three different powder compositions: Al₂O₃ (100%) and Al₂O₃-TiO₂ (97-3 %, 87-13 % and 60-40 %) by plasma spray method in open atmosphere. The microstructures and their formation mechanisms during spraying were discussed. The operation parameters such as carrying gas rate, powder feeding rate and gun velocity were kept constant. Uniform and dense coating layers which are harder 3-4.5 times of the substrate were obtained. XRD results revealed that the coating with pure Al₂O₃ contained some α -Al₂O₃ and mainly γ -Al₂O₃ phases while the layers with TiO₂ particles contained Al₂TiO₅ and TiO₂ (rutile) phases together with α -Al₂O₃ and γ -Al₂O₃ phases.

Acknowledgements

The authors would like to acknowledge Firat University, Turkey for the financial support (Project No. FUBAP-2066). The authors are grateful to Mr. Salih KILINC and Metal & Ceramics Coating Industry Company for providing plasma spraying and powders used in this study.

References

- [1] E. P. Song, B. Hwang, S. Lee, N. J. Kim, J. Ahn, *Materials Science and Engineering A* **4291**, 189 (2006).
- [2] E. P. Song, J. Ahn, S. Lee, N. J. Kim, *Surface and Coatings Technology* **201**, 1309 (2006).
- [3] M. Harju, E. Levänen, T. Mäntylä, *Applied Surface Science* **252**, 8514 (2006).
- [4] M. Bounazef, S. Guessasma, G. Montavon, C. Coddet, *Materials Letters* **58**, 2451 (2004).
- [5] M. F. Morks, K. Akimoto, *Journal of Manufacturing Processes* **10**, 1 (2008).
- [6] M. Wang, L. L. Shaw, *Surface and Coatings Technology* **202**, 34 (2007).
- [7] F.-I. Trifa, G. Montavon, C. Coddet, *Surface and Coatings Technology* **195**, 54 (2005).
- [8] L. L. Shaw, D. Goberman, R. Ren, M. Gell, S. Jiang, Y. Wang, T. D. Xiao, P. R. Strutt, *Surface and Coatings Technology* **130**, 1 (2000).
- [9] E. H. Jordan, M. Gell, Y. H. Sohn, D. Goberman, L. Shaw, S. Jiang, M. Wang, T. D. Xiao, Y. Wang, P. Strutt, *Materials Science and Engineering A* **301**, 80 (2001).
- [10] I. M. Kusoglu, E. Celik, H. Cetinel, I. Ozdemir, O. Demirkurt, K. Onel, *Surface & Coatings Technology* **200**, 1173 (2005).
- [11] B. Liang, G. Zhang, H. Liao, C. Coddet, C. Ding, *Surface & Coatings Technology* **203**, 3235 (2009).
- [12] J. H. Ouyang, S. Sasaki, K. Umeda, *Surface and Coatings Technology* **137**, 21 (2001).
- [13] O. Sarikaya, *Surface & Coatings Technology* **190**, 388 (2005).
- [14] M. F. Morks, K. Akimoto, *Journal of Manufacturing Processes* **10**, 1 (2008).
- [15] H. Luo, D. Goberman, L. Shaw, M. Gell, *Materials Science and Engineering A* **346**, 237 (2003).
- [16] B. Fervel, C. Normand, C. Coddet, *Wear* **230**, 70 (1999).
- [17] Z. Yin, S. Tao, X. Zhou, C. Ding, *Journal of the European Ceramic Society* **28**, 1143 (2008).
- [18] E. P. Song, J. Ahn, S. Lee, N. J. Kim, *Surface and Coating Technology* **202**, 3625 (2008).
- [19] C. J. Li, W. Z. Wang, *Materials Science and Engineering A* **386**, 10 (2004).
- [20] S. Yilmaz, *Ceramics International* **35**, 2017 (2009).
- [21] F. Vargas, H. Ageorges, P. Fournier, P. Fauchais, M. E. Lopez, *Surface and Coatings Technology* **205**, 1132 (2010).
- [22] X. Lin, Y. Zeng, X. Zhou, C. Ding, *Materials Science and Engineering A* **357**, 228 (2003).
- [23] X. Lin, Y. Zeng, S. W. Lee, C. Ding, *Journal of the European Ceramic Society* **24**, 627 (2004).
- [24] D. Wang, Z. Tian, L. Shen, Z. Liu, Y. Huang, *Surface and Coatings Technology* **203**, 1298 (2009).
- [25] W. Tian, Y. Wang, Y. Yang, *Tribology International* **43**, 876 (2010).
- [26] I. Gurappa, *Surface and Coatings Technology* **161**, 70 (2002).
- [27] S. Yugeswaran, V. Selvarajan, M. Vijay, P. V. Ananthapadmanabhan, K. P. Sreekumar, *Ceramics International* **36**, 141 (2010).
- [28] G. Bolelli, V. Cannillo, L. Lusvardi, T. Manfredini, *Wear* **261**, 1298 (2006).
- [29] A. Rico, J. Rodriguez, E. Otero, P. Zeng, W. M. Rainforth, *Wear* **267**, 1191 (2009).
- [30] S. Hoffmann, S. T. Norberg, M. Yoshimura, *Journal of Electroceramics* **16**, 327 (2006).
- [31] C. J. Li, G. J. Yang, A. Ohmori, *Wear* **260**, 1166 (2006).
- [32] G. Sundararajan, D. Sen, G. Sivakumar, *Wear* **258**, 377 (2005).
- [33] W. Tian, Y. Wang, Y. Yang, *Tribology International* **43**, 876 (2010).
- [34] T. Kohara, H. Tamagaki, Y. Ikari, H. Fujii, *Surface and Coating Technology* **185**, 166 (2004).
- [35] V. P. Singh, A. Sil, R. Jayaganthan, *Materials and Design* **32**, 584 (2011).

*Corresponding author: serkanislak@gmail.com